# Numerical Simulation of Convective Diffusion in Blood Flowing in a Channel with a Steady, Three-Dimensional Velocity Field

**M. H. WEISSMAN and T. K. HUNG**

**Carnegie-Mellon University, Pittsburgh, Pennsylvania**

**A numerical study was performed to investigate improvement in mass transfer rates obtainable by introduction of secondary convection into a proposed membrane blood oxygenator. The three-dimensional Navier-Stokes equations were solved numerically for the velocity field in channel and the results used in the numerical solution for the local $P_{O_2}$ in the oxygenator. The convective diffusion equation solved is nonlinear, in addition to being three-dimensional, because of the presence of red cell oxygen sinks.**

**The convection introduced was generated by moving one wall of the blood flow channel laterally to the main flow. Decreases in blood side film resistance up to $5 \times 10^4$ were predicted. In the presence of moderate to strong convection, the limiting factor on oxygenation rate is imposed by the membrane situated between blood and gas phases. It appears that a considerable decrease in required blood priming volume would be possible if the method discussed here were implemented.**

The current thrust in blood oxygenator design is towards more efficient membrane oxygenators. Experience has shown that poor mass transfer efficiency is a major difficulty in many existing membrane oxygenators, and for this reason efficient, nonmembrane devices are sometimes preferred (*1* to *5*). Because membrane oxygenators seem to cause much less damage to the blood than other types, there is an impetus to improve them, and a number of experimental and theoretical demonstrations of improved mass transfer efficiency, obtained through introduction of secondary currents in the blood, have recently been made (*6* to *8*). Convection has a more pronounced effect on oxygen exchange in blood than on other nonreactive fluids, such as water, because the suspended erythrocytes act as sinklike carriers of oxygen.

The designer of a membrane oxygenator strives to maximize oxygen and carbon dioxide transfer rates and thereby to minimize priming volume for a given membrane area. Reflection indicates that the best possible design will be one in which all diffusional resistance is contributed by the membrane, and that of the fluid is made inconsequentially small. In this manner, efficiency will be limited only by the properties of the best available membrane. Currently, this membrane is 1 mil thick, dimethyl silicone rubber, and is about twenty times more permeable to oxygen than is a blood film of equal thickness (*9*).

In striving for optimal design, two strategies may be used effectively: either the blood film thickness may be made extremely small or the blood film diffusion resistance may be annihilated by introduction of strong secondary convection. Several clinical oxygenators have been built by using thin blood films; however, none of these oxygenators has sufficiently diminished blood-side resistance. Membrane support and blood distribution have posed serious difficulties (*10, 11*).

If blood is made to flow in a long, uniform channel of arbitrary cross section, convection may be introduced by using the membrane, which separates blood and gas phases, as a moving wall (see Figure 1*a*). The wall moves at right angles to the axial flow, and the intensity of the convection introduced may be varied continuously through variation of the wall velocity. [Such a scheme might be implemented by cutting a number of identical, parallel channels on a large diameter circular cylinder and by wrapping a closed, cylindrical membrane about it (see Figure 1*b*)]. The membrane, supported by a plastic, porous foam backing, is rotated around the cylinder. Mechanical design problems involved in construction of a cylindrical rotating membrane oxygenator are not considered here.

The optimum shape for the channel, that is, that leading to maximum convection to cross-sectional area ratio for a given membrane speed, is not obvious, and a uniform rectangular channel with a 2:1 aspect ratio was taken as a first approximation. This channel shape simplifies the resultant numerical analysis and is qualitatively representative of the flow behavior observed in an arbitrarily shaped channel.

Two limiting cases of mass transfer are of special interest: that in which fluid resistance is nil and all resistance is due to the membrane (called the *membrane limited case*), and the inverse problem involving a membrane offering no diffusional resistance (called the *fluid limited case*). If the membrane and fluid mass transfer limits differ substantially (that is, mass transfer rate predicted by one limit is three or four times greater than that

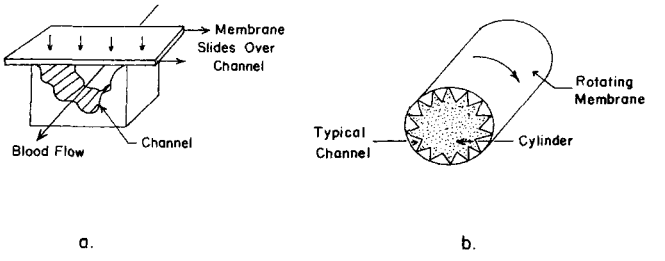


**Fig. 1. Illustrative sketch of convection inducing scheme.**

predicted by the other), the limit predicting the more conservative (slower) mass transfer rate will be close to the true rate. If the two limits are nearly equal, a more general problem, considering presence of both membrane and fluid, must be solved to predict mass transfer accurately. The fluid limiting case has been solved for a range of convection magnitudes, including no convection as a special case.

## THE FLUID LIMIT

The differential equation describing the partial pressure of oxygen in the plasma is (see Figure 2 for definition sketch)

$$D_{O_2,B}\left[\frac{\partial^2 P_{O_2}}{\partial x^2}+\frac{\partial^2 P_{O_2}}{\partial y^2}+\frac{\partial^2 P_{O_2}}{\partial z^2}\right] = [1+f(P_{O_2})]\left[u\frac{\partial P_{O_2}}{\partial x}+v\frac{\partial P_{O_2}}{\partial y}+w\frac{\partial P_{O_2}}{\partial z}\right] \quad (1)$$

where $f(P_{O_2})$ is of the form $ae^{-bP_{O_2}}+ce^{-(dP_{O_2}+g)}$ (12).

This equation differs from simple convection diffusion equations, as it contains an empirically evaluated chemical reaction term $f(P_{O_2})$. The primary assumption in the derivation of this term is that the blood plasma and red blood cells are in equilibrium with respect to oxygen content. Additionally, partial pressures are written instead of concentrations, as Henry's law applies for oxygen in plasma (16).

The oxygen equation is put in a useful dimensionless form by introduction of the dimensionless variables

$$U=\frac{u}{u_b},\quad V=\frac{v}{u_b},\quad W=\frac{w}{\frac{L^2}{\mu}\left(\frac{\partial p}{\partial z}\right)}$$

$$X=\frac{x}{L},\quad Y=\frac{y}{L},\quad Z=\frac{z}{LN_K}$$

The dimensionless axial and convective velocities are referred to separate reference quantities because they are generated independently of each other by separate driving forces. Introduction of the dimensionless variables in the oxygen equation leads to the form

$$\frac{\partial^2 P_{O_2}}{\partial X^2}+\frac{\partial^2 P_{O_2}}{\partial Y^2}+\frac{1}{N_K^2}\frac{\partial^2 P_{O_2}}{\partial Z^2} = [1+f(P_{O_2})]N_{Sc}\left[N_{Reb}\left(U\frac{\partial P_{O_2}}{\partial X}+V\frac{\partial P_{O_2}}{\partial Y}\right)+W\frac{\partial P_{O_2}}{\partial Z}\right] \quad (2)$$

in which

$$N_K=L^3\rho\frac{\partial p}{\partial z}\Big/\mu^2$$

$$N_{Reb}=\frac{u_bL\rho}{\mu},\ \text{the lateral Reynolds number}$$

$$N_{Sc}=\left(\frac{\mu}{\rho D_{O_2,B}}\right),\ \text{the Schmidt number}$$

$$P_{O_2}=P_{O_2}(X,Y,Z)$$

Some simplification results from neglecting the axial diffusion term, which is small. The equation remains three-dimensional and nonlinear even so.

The initial and boundary conditions associated with Equation (2) are

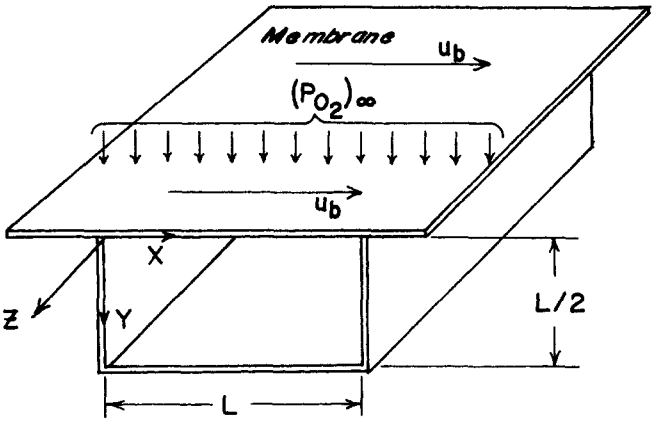


Fig. 2. Definition sketch for this study.

@ $Z=0$: $P_{O_2}(X,Y,0)=(P_{O_2})_0$, the initial oxygen tension in the blood,

@ $Y=0$: $P_{O_2}(X,0,Z)=(P_{O_2})_\infty$, the value of oxygen tension in the atmosphere (zero membrane resistance),

@ $X=0,1$: $\frac{\partial P_{O_2}}{\partial X}(0,Y,Z)=\frac{\partial P_{O_2}}{\partial X}(1,Y,Z)=0$

@ $Y=\frac{1}{2}$: $\frac{\partial P_{O_2}}{\partial Y}(X,\frac{1}{2},Z)=0$ (3)

The last conditions, at $X=0$ and 1 and $Y=\frac{1}{2}$, are appropriate to impermeable channel walls and imply no oxygen flux at the wall.

## NUMERICAL SOLUTION

Solutions to the above boundary-value problem may be obtained numerically provided that the velocity field is known. Unfortunately, analytic solutions for the velocity field are not available, and velocities must be obtained from numerical solution of the three-dimensional equations of fluid motion before the oxygenation problem may be solved. Although blood is non-Newtonian, the Navier-Stokes equations were used for a first approximation of the equations of motion, since a general constitutive equation for blood is not now known. A value of 4750 was used for $N_{Sc}$.

The method used to obtain the three-dimensional velocity field, under a uniform flow situation, is the subject of another paper (14); however, typical results are illustrated here. Figure 3 shows streamlines for the convection velocities in the channel cross section in the case $N_{Reb}=100$. Since the channel is long, the velocities are assumed to be fully developed (no variation in the axial direction). The dimensionless axial velocities were found to have similar profiles [that is, they depend on $N_{Reb}$ but not on $(\partial p/\partial z)$]. Figure 4 shows the dimensionless axial velocity profile for $N_{Reb}=100$; this may be contrasted with the symmetric axial velocity profile obtained for $N_{Reb}=0$ (no convection). Introduction of a lateral membrane velocity has only a second-order effect on the discharge for a fixed axial pressure gradient (14).

The newly obtained velocity distributions were used in conjunction with the convective diffusion equation for oxygen in plasma, and the equation solved numerically.

The differential equation was simulated by 169 implicit, upwind, difference equations on a grid of 169 rectangularly symmetric points. One solution with a 676 point grid was performed to check the accuracy of the 169 point solutions. This solution made use of a finer grid to obtain more accurate velocities, as well as a finer grid for the numerical solution of the diffusion equation.

Upwind (may be either forward or backward) differences were used in the simulation, since stability criteria for a central difference representation require very small grid spacing in the presence of large convection velocities. A very fine grid makes computer solution time impractically long. Consistent use of upwind differences leads, in problems with significant convection, to difference equations having small, nonnegative coefficients, such that the sum of the absolute values of the coefficients of the surrounding grid points does not exceed that of the point for which the equation is written. This situation, in turn, leads to stability in an iterative solution (*15*). Difference equations were solved by using an improved relaxation method, and the solution accuracy was increased by use of linear Richardson extrapolation. A relative error of 1 part in $10^6$ was used as a convergence criterion for the relaxation. Halving the convergence criterion did not affect the solution in any way, except by increasing computer time very slightly.

Solutions were obtained corresponding to $N_{Reb} = 0$, 5 and 100. Several values of $(P_{O_2})_\infty$ were used, whereas only one value for $(P_{O_2})_0$ was used. In reporting blood oxygenation research, it is common to present solutions in terms of oxygen saturation, rather than partial pressure. Oxygen saturation is defined as the percent of the total oxygen carrying capacity of the red blood cells which is being utilized, and is related to $P_{O_2}$ through the empirically determined oxy-hemoglobin dissociation curve (*16*).

In the absence of secondary velocity $N_{Reb} = 0$ (that is, the case of no membrane motion), the surfaces of constant oxygen saturation in the blood are symmetric with respect to the vertical midplane of the channel, $X = 0.5$. Figure 5 shows cross-sectional views of these surfaces, in the $X$-$Y$ plane, at various distances downstream. In cross section the surfaces appear as contour lines of constant oxygen saturation. Contour plots, obtained from the 169 point solution, are drawn for average (cup mixing) saturations of 80, 85, 90 and 95% in Figure 5. On each plot, contours of constant oxygen saturation are shown at 2.5% intervals from 77.5 to 97.5%. The initial oxygen partial pressure was taken as 54 mm. Hg, a normal value for venous blood, which corresponds to 75% venous oxygen saturation. The value for $(P_{O_2})_\infty$ was taken as 150 mm. Hg in these solutions (normal atmospheric value) and resulted in a maximum oxygen saturation of 100%. The horizontal line on top of each drawing in Figure 5 represents not only the upper boundary of the channel, but also the 100% saturation contour.

At any given depth $Y$ in the channel, the axial velocity is always a maximum on the midplane $X = 0.5$. It would be expected that blood which travels quickly through the channel would take up less oxygen than blood travelling slowly. This behavior is seen clearly in Figure 5 in that the greatest oxygen penetration, at a given depth, occurs at the vertical side walls, where the velocity is zero, and the least at $X = 0.5$, where the velocity is greatest.

The addition of secondary velocity changes the symmetric contours of Figure 5 to those shown in Figure 6, for $N_{Reb} = 100$. Well-oxygenated blood from the surface is drawn into the interior of the channel by the secondary flow. This convected blood sweeps through the channel in a counter clockwise direction and eventually returns near the upper surface, where it meets another mass of well-oxygenated blood and forms closed oxygen saturation contours (Figure 6*b*, *c*, *d*). The nodes, or the centers of the closed contours, in Figure 6 are the last places to be reached by the oxygen and are located at the points where the secondary velocity is zero. The node in Figure 6 corresponds exactly to the node of the streamlines shown in Figure 3.

Presence of red blood cells, with their chemical affinity for oxygen, aids the oxygenation process by helping to maintain a steep oxygen gradient near the membrane in

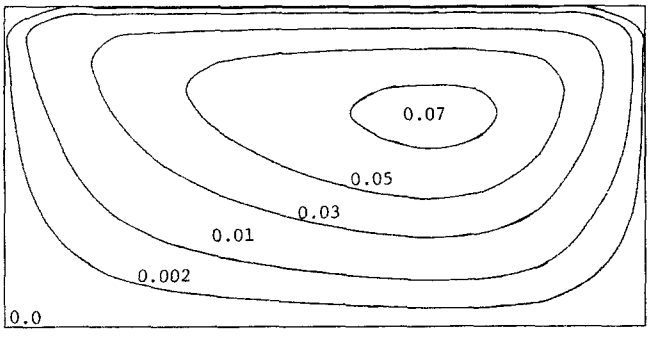


Fig. 3. Streamlines for secondary velocities in X-Y plane for $N_{Reb} = 100$. Stream function values noted as curves.

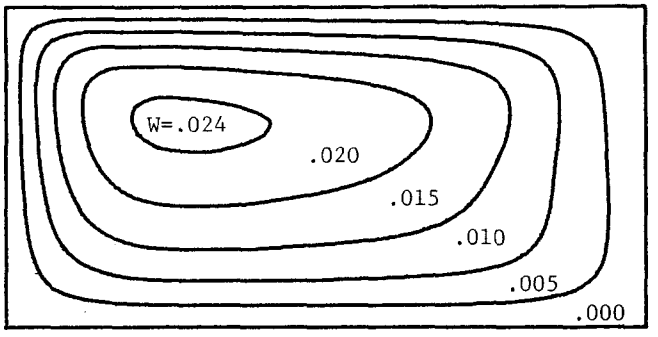


Fig. 4. Constant dimensionless axial velocity curves; lateral Reynolds number equals 100. Contour interval is one-tenth of maximum axial velocity.

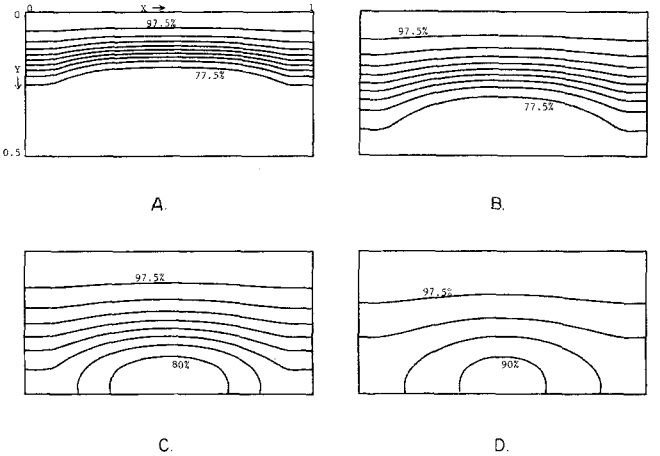


Fig. 5. Oxygen saturation contour lines for $N_{Reb} = 0$. Contour interval is 2.5% $(P_{O_2})_\infty$ equals 150 mm. Hg. Topmost contour line represents 97.5%. A: Saturation increase is 5%, B: 10%, C: 15%, D: 20%. Initial saturation is 75%.

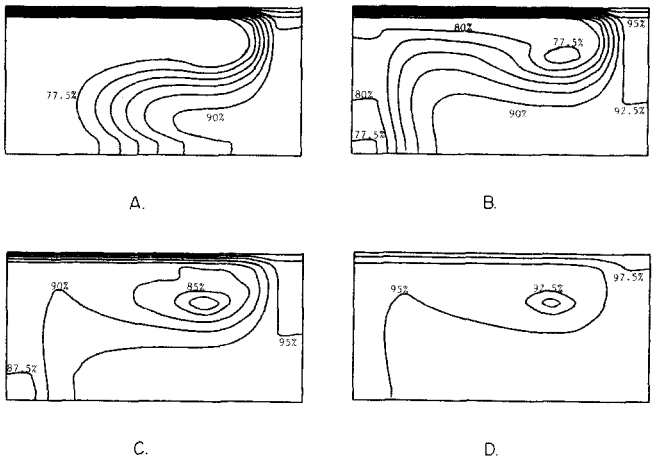


**Fig. 6. Saturation contour lines for $N_{Reb} = 100$. Contour interval is 2.5%; $(P_{O_2})_\infty$ equals 150 mm. Hg. Topmost contour line represents 97.5%. A: Saturation increase is 5%, B: 10%, C: 15%, D: 20%. Initial saturation is 75%.**

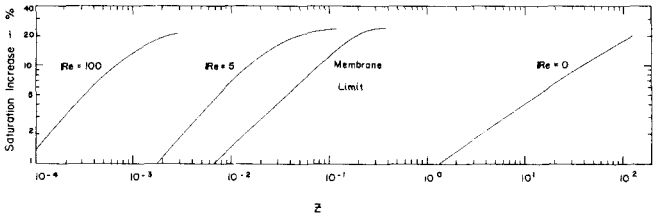


**Fig. 7. Average oxygen saturation increase vs. dimensionless axial length; $(P_{O_2})_\infty$ equal to 150 mm. Hg.**

the blood and also by increasing the amount of oxygen which can be unloaded in the channel interior. Contours for the case $N_{Reb} = 5$ are qualitatively similar to those shown in Figure 6.

The increase in average saturation as a function of $Z$ is shown in Figure 7 for $N_{Reb} = 0$, 5, 100, and for $(P_{O_2})_\infty =$ 150 mm. Hg. Figure 7 also shows, by way of example, the membrane limit for a channel with membrane thickness to channel depth ratio of 1:125, with a silicone rubber membrane of diffusivity $D_{O_2,m}$, $1.60 \times 10^{-5}$ cm./sec., and a blood kinematic viscosity of 0.04 sq.cm./sec. [The membrane limit was obtained previously in terms of a dimensionless axial length $z^*$, equal to $\left(\frac{D_{O_2,m}L^2}{t^2 \nu \overline{W}}\right)$ times the Z of this paper (*17*)].

Note that whereas the membrane limit is area-dependent, the fluid limit does not depend on the size of the channel cross section, but only its shape. Note also that for a 2:1 rectangular channel the pressure gradient is related to the blood flow rate $Q$ by $\partial p/\partial z = Q\mu/L^4k$, where the constant $k$ is 0.0035 for $N_{Reb} = 0$ and decreases slightly as $N_{Reb}$ rises (*14*). Thus $Z$ is also equal to $kN_{Sc}ZDo_{2,b}/Q$.

In the absence of secondary convection, the factor limiting the oxygenation rate in the example channel is clearly the diffusional resistance of the blood film. The fluid limit lies nearly three orders of magnitude to the right of the membrane limit, for this case, indicating that the oxygenation rate is not sensitive to membrane thickness. With the introduction of strong convection, the fluid limit curves are shifted far to the left of the membrane limit. For this situation, the limiting factors on oxygenation are the composition and thickness of the membrane. The fluid side resistance to diffusion decreases by a factor of $5 \times 10^4$ in going from $N_{Reb} = 0$ to $N_{Reb} = 100$.

Figure 8 illustrates the effect of increasing $(P_{O_2})_\infty$ for the case $N_{Reb} = 100$. It can be seen that a law of diminishing returns applies when $(P_{O_2})_\infty$ is increased, since the channel length needed for a given saturation increase can be seen to decrease more slowly than the initial difference $[(P_{O_2})_\infty - (P_{O_2})_0]$ increases.

Also shown in Figure 8 are results from a solution using a 676 point grid, a $P_{O_2}$ of 750 mm. Hg, and Reynolds number of 100 ($X$ and $Y$ grid spacing both halved). Comparison of the 169 and 676 point solutions shows that a difference of about 30% exists between the two. This difference, while large in an ordinary sense, is relatively unimportant when comparing results which differ by many orders of magnitude (five orders of magnitude between solutions for $N_{Reb} = 100$ and $N_{Reb} = 0$). The example chosen for more accurate solution represents a worse case, and at Reynolds numbers and $(P_{O_2})_z$'s less than 100 and 750, respectively, error will be much less than 30%, decreasing to nearly zero at $N_{Reb} = 0$ (*6, 17*).

Saturation profiles for the more accurate solution are qualitatively similar to those obtained with a coarser grid, with the exception that the interface between oxygenated and venous blood is slightly sharper. This comparative behavior is shown in Figure 9 for a 10% average saturation increase $[(P_{O_2})_\infty = 750, N_{Reb} = 100]$. Figure 10 shows behavior of the average saturation solution curves for $N_{Reb} = 5$ and various values of $(P_{O_2})_\infty$, while Figure 11 shows the same for $N_{Reb} = 0$. Results are qualitatively similar to those for the case $N_{Reb} = 100$.

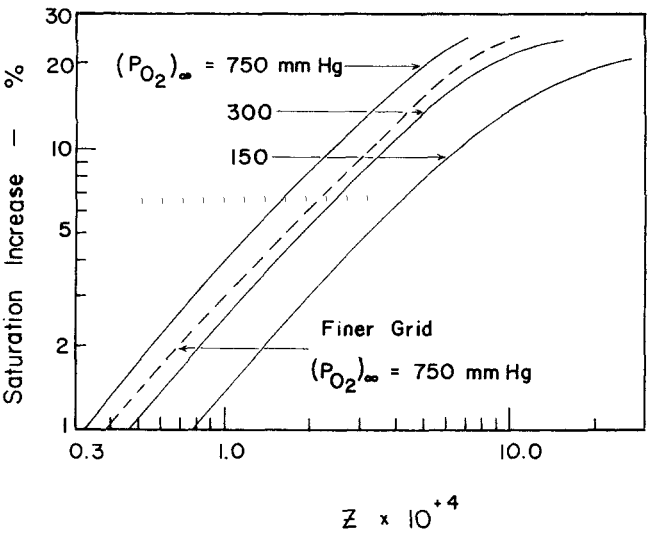


**Fig. 8. Average oxygen saturation increase vs. dimensionless axial length Z, for constant Reynolds number $N_{Reb} = 100$; $(P_{O_2})_z$ is varied.**

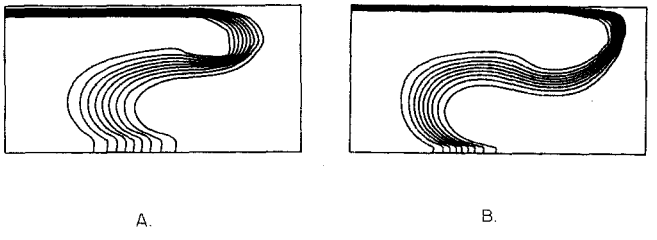


**Fig. 9. Oxygen saturation contours for $N_{Reb} = 100$ and $(P_{O_2})_\infty =$ 750 mm. Hg. A: 169 point solution, B: 676 point solution. Contour interval is 2.5%, topmost contour is 97.5%. Initial saturation is 75%.**

It is currently impractical to decrease grid spacing further, as halving the grid spacing increases computation time by a factor of about 13. (For example, the 169 point solution required 3.6 min. on a Univac 1108 computer, whereas the corresponding 676 point solution took 46 min., plus an extra 40 min. needed to obtain the more accurate velocities.)

## CONCLUSIONS AND DISCUSSION

Results of this study indicate clearly that introducing active secondary circulation is an effective method of reducing blood film resistance to minimal levels. Reductions can be obtained which suffice to allow the dominance of the membrane limit for the best currently available membrane. For the membrane/channel geometry chosen here as an example, the lateral Reynolds number for the secondary flow must be of the order of 5, to reach the membrane limiting situation. Discretization error in the numerical solutions is not negligible; however, it is not excessive in a comparative sense. At present, use of finer grids for more accurate solutions is not feasible because of the long computer time required.

It has been noted previously that for a membrane limited oxygenator, the membrane area is independent of channel size and geometry, but the priming volume is proportional to the channel width $L$ (*17*). Thus, the priming volume may be reduced as desired by using small channels. The price paid for this reduction in priming volume is the necessity for higher lateral velocities, $u_b$ becoming infinite as the priming volume goes to zero. Higher velocities are needed since, for a fixed lateral Reynolds number, $u_b$ is inversely proportional to $L$.

It is difficult to predict, a priori, the extent of the blood trauma which might be generated in a moving membrane oxygenator without performing actual experiments. However, if the shear rate can be used as an index of probable damage, the secondary flow will not be excessively traumatic. For example, in a channel of width 0.125 in., at a lateral Reynolds' number of 100, the maximum shear rate caused by the secondary flow is of the order of 250 sec.$^{-1}$, a relatively small value.

The present work offers no clues as to an optimum channel shape; however, the use of triangular channels would lead to a decrease in priming volume, while not effecting membrane area. It would appear possible, by using a triangular channel (with a maximum depth of 0.0625 and a maximum width of 0.125 in.), to build an oxygenator with a blood flow capacity of 5 liters/min. and a priming volume of 460 cc., which would provide a 20% saturation increase and have a normal ratio of oxygen to carbon dioxide flow, while using an atmospheric $(P_{O_2})_\infty$ of 300 mm. Hg (*17*). Such operating characteristics are highly desirable from a clinical standpoint (*1*).

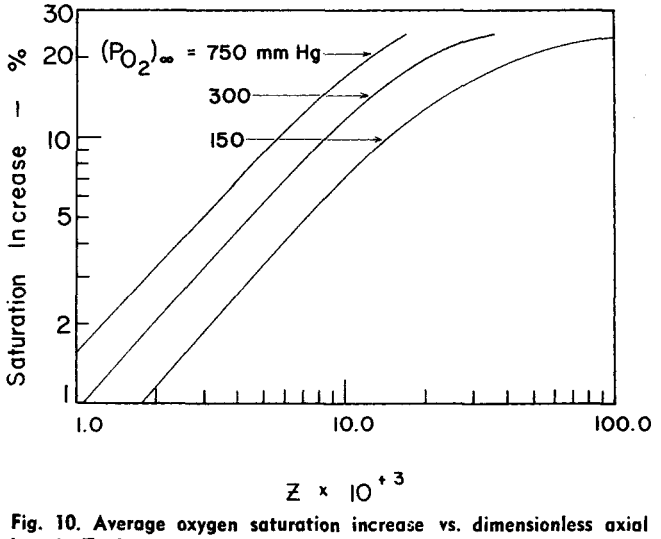


Fig. 10. Average oxygen saturation increase vs. dimensionless axial length Z, for constant Reynolds number, $N_{Re_b} = 5$, $(P_{O_2})_\infty$ is varied.

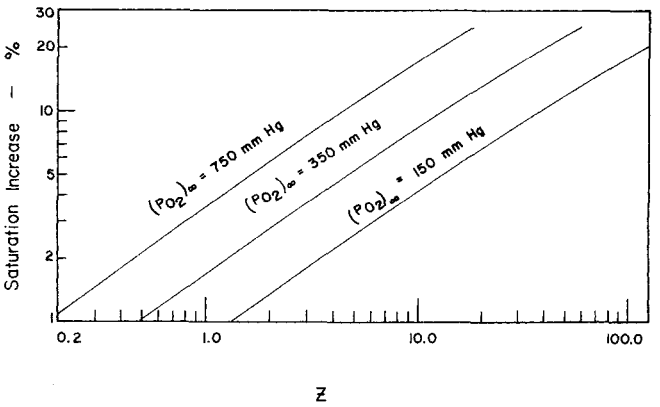


Fig. 11. Average oxygen saturation increase vs. dimensionless axial length Z, for constant Reynolds number, $N_{Re_b} = 0$, $(P_{O_2})_\infty$ is varied.

The oxygenation rate could be improved if $(P_{O_2})_\infty$ were raised further, but carbon dioxide elimination would then become a problem. The above estimate is slightly optimistic, as no account is taken of the entrance length for the velocity profile, which is not known. However, for laminar flow one might expect an entrance length of not more than 5 or 10 channel widths at Reynolds number 100 (in analogy with inlet lengths in round pipes).

It appears theoretically possible to optimize membrane oxygenator design of introduction of strong secondary convection leading to increased mass transfer efficiency. Such optimization can lead to a clinically acceptable membrane oxygenator. The conclusions of this study currently await experimental verification.


## ACKNOWLEDGMENT

The authors wish to thank the Carnegie-Mellon University Computation Center for their generous donation of the computer time needed to complete this study.


## NOTATION

$D_{O_2,B}$ = effective diffusivity of oxygen in whole blood
$D_{O_2,m}$ = diffusivity of oxygen in polymeric membrane
$f(\ )$ = oxygen sink function
$k$ = constant
$L$ = channel width
$N_K$ = Karman number, equal to $L^3 \rho \frac{\partial p}{\partial z}/\mu^2$
$N_{Re_b}$ = lateral Reynolds number
$N_{Sc}$ = Schmidt number
$p$ = hydrostatic pressure
$P_{O_2}$ = partial pressure of oxygen in blood plasma
$Q$ = blood flow rate
$t$ = membrane thickness
$u_b$ = membrane lateral velocity
$u, v, w$ = dimensional velocities in $x, y, z$ directions
$U, V, W$ = dimensionless velocities
$\overline{w}$ = average dimensional axial velocity

$\overline{W}$ = average dimensionless axial velocity
$x, y, z$ = orthogonal Cartesian coordinates
$X, Y, Z$ = dimensionless coordinates
$\partial p/\partial z$ = hydrostatic axial pressure gradient
$\mu$ = dynamic viscosity of blood, [the viscosity may be taken as a constant at shear rates exceeding 50 to 100 sec.$^{-1}$. At lesser shear rates, blood is non-Newtonian and is adequately described by the Casson equation (13)]
$\nu$ = kinematic viscosity of blood
$\rho$ = density of blood
$( )_\infty$ = condition at $Y = 0$
$( )_0$ = condition at $Z = 0$

## LITERATURE CITED


1. Galleti, P. M., and G. A. Brecker, "Heart Lung Bypass," Grune and Stratton, New York (1962).
2. Esmond, W. G., et al., *Proc. ACEMB*, **10**, No. 12, 5 (1968).
3. Cross, F. S., et al., *Surgical Forum*, **7**, No. 427 (1956).
4. Gibbon, J. H., Jr., et al., *Medical Clinics of North America*, **37**, 1603 (1953).
5. Cooley, D. A., *et al., Surgery*, **52**, 713 (1962).
6. Weissman, M. H., and L. F. Mockros, *J. Eng. Mech. Div.*, **94**, 857 (1968).
7. Drinker, P. A., et al., Paper presented at 1968 Am. Soc. Civil Engrs., Annual Meeting, Pittsburgh, Pa. (Sept., 1968).
8. Keller, K. H., *Progress Report on PHS Contract 43671419, NHI* (1969).
9. Robb, W. L., *General Electric R&D Center Report 65-C-031* (Oct., 1965).
10. Gerbode, Frank, et al., *Am. J. Surgery*, **114**, 16 (1967).
11. Peirce, E. C., II, *Surgery*, **52**, 777 (1960).
12. Weissman, M. H., and L. F. Mockros, *J. Eng. Mech. Div.*, **93**, 225 (1967).
13. Merrill, E. W., et al., *J. Appl. Physiol.*, **20**, 954 (1965).
14. Hung, T. K., and M. H. Weissman, M.S. in preparation.
15. Young, David, *Trans. Am. Math. Soc.*, **76**, 92 (1954).
16. Ruch, T. C., and J. F. Fulton, "Medical Physiology and Biophysics," W. B. Saunders, Philadelphia, Pa. (1960).
17. Weissman, M. H., *AIChE J.*, **15**, 627 (1969).


*Manuscript received March 5, 1969; revision received May 1, 1969; paper accepted May 5, 1969.*

# Optimal Operation of a Variable-Volume Stirred Tank Reactor

**MONTY M. LUND and RICHARD C. SEAGRAVE**

**Iowa State University, Ames, Iowa**

**For certain classes of chemical reactions, it is possible to increase the yield of the desired products by choosing appropriate variable-volume operating policies. An analysis of the steady state and semibatch operation of a stirred tank reactor demonstrates operating policies for both the isothermal and adiabatic case to maximize the steady state yield and to produce an improved semibatch yield. Computations carried out by using an analogue computer with a digital logic expansion system demonstrate further relationships between yield increase and operating policy.**

The continuous stirred tank or backmixed reactor is a very common chemical engineering processing unit. A considerable amount of analysis regarding the design, operation, and control of these units has produced much useful information for engineers (*1, 9*). Generally, these reactors are operated at or near steady state, with the mean residence time adjusted to produce the optimum or desired product yield. It has been observed (*7*) that in selected cases the value of an increased yield which might be obtainable from a periodic operating policy would be enough to offset the additional costs resulting from increased handling and storage. In order to investigate the economic feasibility of such schemes, it is necessary to quantitatively investigate the relationships between the yield of a backmixed reactor and the operating variables encountered during variable-volume operation. The concept of increasing the yield of a chemical reactor by various types of periodic operation is becoming of interest to chemical engineers (*3* to *8*). However, the variable-volume periodic reactor has been neglected, although the concept of a variable-volume periodic reactor abounds in nature, perhaps the foremost example being the human lung.

In this work, analysis is carried out on isothermal and adiabatic stirred tank reactors. These two extreme or limiting cases represent a logical starting point but by no means cover the entire range of operating conditions found in practice. Although it appears that the possible obtainable improved yield for a periodic operation will be more dramatic for higher order reactions, this study concentrates on the irreversible first-order reaction. The techniques of analysis are easily extendable to higher-order reactions. This approach is justified on two counts, the one being that a very large class of reactions may be treated at least as pseudo first-order reactions, and the other being the simplicity of the case which hopefully results in increased insight into the overall situation of variable-volume operation.

While the isothermal case is almost completely amenable to analytical solution, the adiabatic case requires the use of an analogue computer with an associated digital logic expansion system to solve the working equations and to provide some insight into the factors influencing the relationships between yield increase and operating policy.

The following general equations may be written for a completely backmixed stirred tank reactor as depicted in Figure 1, assuming negligible volume change due to chemical reaction, but not necessarily operating at constant volume.

Monty M. Lund is with The Dow Chemical Company in Midland, Michigan.